A spectral-domain wave-to-wire model of wave energy converters

Tan, Jian; Tao, Wei; Laguna, Antonio Jarquin; Polinder, Henk; Xing, Yihan; Miedema, Sape

DOI
10.1016/j.apor.2023.103650

Publication date
2023

Document Version
Final published version

Published in
Applied Ocean Research

Applied Ocean Research 138 (2023) 103650

Contents lists available at ScienceDirect

Applied Ocean Research

journal homepage: www.elsevier.com/locate/apor

Invited paper

A spectral-domain wave-to-wire model of wave energy converters

Jian Tan [a,d], Wei Tao [b,a,*], Antonio Jarquin Laguna [a], Henk Polinder [a], Yihan Xing [c], Sape Miedema [a]

[a] Department of Maritime & Transport Technology, Delft University of Technology, The Netherlands
[b] School of Mathematics and Computer Science, Wuhan Polytechnic University, China
[c] Department of Mechanical and Structural Engineering and Materials Science, University of Stavanger, Norway
[d] VOSTA LMG, The Netherlands

ARTICLE INFO

Keywords:
Wave energy converter
Spectral-domain modeling
Wave-to-wire model

ABSTRACT

Wave-to-Wire models play an important role in the development of wave energy converters. They could provide insight into the complete operating process of wave energy converters, from the power absorption stage to the power conversion stage. In order to cover a set of relevant nonlinear effects, wave-to-wire models are predominately established in the time domain. However, the low computational efficiency of time-domain modeling is hindering the extensive application of wave-to-wire models, especially in early-stage design and optimization where a large number of iterations are required. To address this issue, a spectral-domain wave-to-wire model is proposed, and the nonlinear effects are incorporated by stochastic linearization. This model can significantly reduce the computational load and maintain good accuracy. The reference concept studied in this paper is defined as a heaving point absorber coupled with a linear permanent-magnet generator. Four representative nonlinear effects involved in both the hydrodynamic stage and the electrical stage of the concept are considered. The proposed model is verified against a corresponding nonlinear time-domain wave-to-wire model, and a good agreement is observed. The relative error of the proposed spectral-domain wave-to-wire model is around 2 % in typical operational regions and is still within 7 % for wave states with large significant wave heights, regarding the estimate of the power conversion efficiency. Meanwhile, the computational load of the spectral-domain wave-to-wire model is reduced by 2 to 3 orders of magnitudes compared with the conventional time-domain approach. Finally, a case study of tuning the PTO damping to maximize power production is conducted to demonstrate the performance of the proposed spectral-domain wave-to-wire model.

1. Introduction

Towards the energy transition, ocean wave energy is expected to play a significant role because of its unique advantages. First, ocean waves carry a considerable amount of clean energy, and the global wave energy resource is estimated to be around 2.11 TW (Gunn and Stock-Williams, 2012). Secondly, ocean wave energy is a kind of continuous energy resource no matter in daytime or nighttime. Thirdly, it is globally distributed, and most counties or regions have access to ocean wave energy. However, compared with wind or solar energy, wave energy is still recognized as a form of untapped renewable energy resource (Gonzalez et al., 2021; Tan et al., 2021a). Numerical modeling plays an important role in the design and optimization of wave energy converters (WECs). This is because it could effectively provide insight into the behavior and performance of WECs at a remarkably lower cost than the experiment. Thus, to accelerate the exploitation and commercialization of wave energy, it is of great importance to further develop numerical modeling.

The most commonly used numerical models in the field of WECs can be classified as frequency-domain (FD) models, time-domain (TD) models and Computational Fluid Dynamics (CFD) models. Their computational efficiency decreases in the sequence, while the fidelity increases. CFD models are a kind of fully nonlinear numerical models, in which Navier–Stokes equations are solved numerically. Navier–Stokes equations are derived from the conservation of mass and momentum and are generally considered to be the most fundamental fluid flow equations. Thus, viscous effects and turbulence are taken into account in CFD models. On the other hand, CFD models are significantly more time-consuming compared to nonlinear TD models, which is the main limitation of the extensive application of CFD models. Therefore, CFD models are mostly used in the assessment of the survivability of WECs in severe wave conditions, but they are hardly used to estimate power production. Instead, the power performance of WECs is usually estimated by FD or TD models.

* Corresponding author at: School of Mathematics and Computer Science, Wuhan Polytechnic University, China.
E-mail address: taowei@whpu.edu.cn (W. Tao).

https://doi.org/10.1016/j.apor.2023.103650
Received 12 February 2023; Received in revised form 8 June 2023; Accepted 24 June 2023
Available online 10 July 2023

In the context of WECs, FD models and TD models are commonly established based on linear potential theory (Penalba Retes et al., 2015). The linear potential flow theory has been used to solve wave-structure interaction problems in offshore engineering over the decades. In the theory, fluid is assumed to be inviscid, irrotational and incompressible, and thus vortexes and viscosity are neglected. In addition, in order to simplify the problem, the boundary conditions of the free surface and body are linearized as the mean free surface and the mean wetted surface. Linear potential flow theory is computationally efficient to derive hydrodynamic coefficients. Given the explicit coefficients, FD models can be formulated according to physical principles to estimate the dynamics of WECs. External forces can be taken into account, but all the components in the conventional FD models are required to be linear. The most important advantage of FD models is their simplicity and thus high efficiency. Further, based on the Cummins equation (Cummins et al., 1962) describing the memory effects of radiation forces, TD models can be established and the time-dependent responses of WECs can be solved. In TD models, nonlinear force components can be incorporated, such as the nonlinear mooring force, power take-off (PTO) machinery force and viscous drag force (Giorgi and Ringwood, 2018; Folley, 2016b). The consideration of nonlinear forces could increase the accuracy of TD modeling, particularly in regions with relatively large displacement and velocity of the captor. Even though TD models are associated with higher fidelity than FD models, the computational demand of TD models is typically several orders of magnitude higher than that of FD model (Tan et al., 2022a). The reason is that TD modeling requires numerical integration schemes to solve partial differential equations in each time step (Ricci et al., 2008).

Wave-to-Wire modeling is a kind of numerical approach to assessing the performance of WECs (Penalba and Ringwood, 2016). It can be used to characterize the complete operation process, covering the wave-buoy hydrodynamics, energy transmission and electricity generation (Folley, 2016b). Thus, the performance of WECs can be systematically analyzed by means of wave-to-wire models. In the last years, various wave-to-wire models have been proposed and validated for different types of WECs. In Ciappi et al. (2022) and Henriques et al. (2019), nonlinear TD wave-to-wire models were established for oscillating water column (OWC) devices, and the applications of different air turbines were considered. The models showed a strong ability to analyze the performance of each system component. As presented in Balitsky et al. (2019), a wave-to-wire model for an oscillating surge wave energy converter (OSWEC) was developed, in which a hydraulic PTO system was employed. In addition, wave-to-wire approaches have also been applied for overtopping WECs (Igic et al., 2011) and attenuator-type WECs (Liu et al., 2021). For point absorbers, a set of recent studies have been dedicated to the development of wave-to-wire models (Penalba and Ringwood, 2019; Penalba et al., 2017c,a; Tan et al., 2023). These models offered a more comprehensive figure of the devices than pure hydrodynamic models. For instance, the PTO parameters of WECs are normally tuned, based on hydrodynamic models, to maximize the absorbed mechanical power by achieving the desired velocity or phase of the floater (Hals et al., 2010; Tan et al., 2020). But it has been indicated in Son and Yeung (2017) and Coe and Bacelli (2023) that the conversion efficiency of electrical generators also has a strong dependence on the PTO parameters. The PTO parameters optimal for the absorption of mechanical power are not necessarily optimal for the production of electrical power. This apparently cannot be revealed with only hydrodynamic models. In addition, the conversion efficiency of the electrical generator in PTO systems is strongly associated with the operating conditions of WECs. It has been shown in Tan et al. (2022b) and Tan et al. (2021b) that the efficiency could differ from around 70% in high-frequency waves to 20% in low-frequency waves for the linear generator applied in a point absorber. Thus, the lack of modeling of the electrical generators might lead to a poor estimate of the actual power performance or the annual energy production (AEP) of WECs. Therefore, it is not sufficient to rely on hydrodynamic models in the design and optimization of WECs. This clearly implies the necessity of developing wave-to-wire models for the relevant analysis. Existing wave-to-wire models are predominately established based on the TD approach with an intention to cover a variety of nonlinear effects in the power absorption, transmission and conversion stages. However, as the technology of WECs still stays in a pre-mature phase, the design and optimization are thus inherently associated with a large number of iterations. Then, using the TD wave-to-wire models would inevitably make the process remarkably time-consuming. Thus, developing more computationally-efficient wave-to-wire models is expected to make a significant contribution to the advance of WECs towards large-scale commercialization.

As a relatively new numerical technique in the field of WECs, spectral-domain (SD) modeling has received research interest in recent years because of its high efficiency. As investigated in Folley and Whittaker (2010) and Tan et al. (2022a), SD modeling is typically thousands of times computationally faster than TD modeling while the relative error is no more than 5% in operational regions. In principle, SD modeling is formulated based on the framework of FD modeling. Comparatively, different from conventional FD modeling, SD modeling allows for the inclusion of nonlinear effects by means of stochastic linearization. The linearization is implemented based on the assumption of Gaussian distribution being valid for WECs as a system. In Folley and Whittaker (2010), SD modeling was applied in the context of WECs for the first time. In the study, the quadratic damping representing the viscous drag force and wave force decoupling due to large amplitudes of the motion were incorporated in the SD modeling of a flap-type WEC. The loads and motion estimated by the SD modeling presented a good agreement with the TD model. In the past years, SD modeling has been further developed to cover the end-stop force, mooring force, viscous drag force, Coulomb damping, nonlinear hydrostatic force and PTO force constraint (Silva, 2019; da Silva et al., 2020; Silva et al., 2020; Spanos et al., 2018; Gunawardane et al., 2017; Tan et al., 2022a). Given its merits, extending SD modeling to cover the whole wave-to-wire process could significantly improve the computational efficiency when analyzing the comprehensive performance of WECs is in demand. An important function of the wave-to-wire models is to reflect the behavior of electrical components whose characteristics are different from hydrodynamic responses. Although the SD modeling has been well verified for predicting the hydrodynamic responses, its applicability still remains unclear with regard to integrating the electrical modeling.

The objective of this paper is to develop a wave-to-wire model purely represented in the spectral domain. A heaving spherical point absorber integrated with a linear permanent magnet (PM) generator and a power converter is considered as the research reference in this work. The established model is able to predict the relevant statistical responses involved not only in the power absorption stage but also in the power conversion stage of WECs. In the power absorption stage, the nonlinear effects of the PTO force saturation, and viscous drag force are taken into account. In the power conversion stage, the first addressed nonlinear effect is the partial overlap between the translator and stator of the linear generator, and the second is the stator current limit. Compared with TD wave-to-wire modeling, the proposed SD wave-to-wire model significantly accelerates the numerical computation. For verification, the results obtained by the proposed SD wave-to-wire model are compared with those from a nonlinear TD wave-to-wire model. Finally, a case study of tuning the PTO damping of WECs is implemented to demonstrate the performance of the proposed SD wave-to-wire model.

2. Concept description

Although it is possible to formulate SD wave-to-wire models for various combinations of captors and PTO systems, this work focuses on a heaving point absorber concept coupled with a linear PM generator. This is because this concept has received a lot of attention in recent

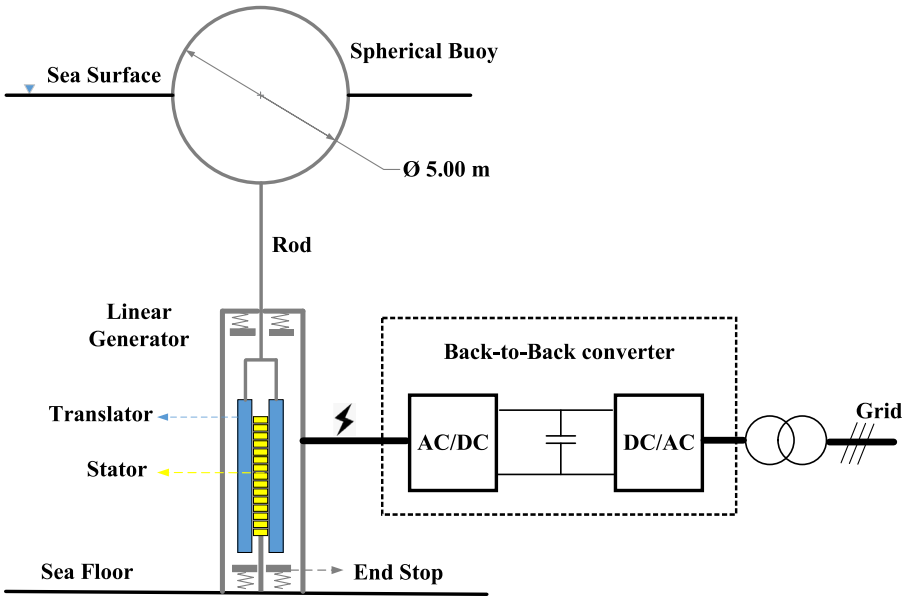

Fig. 1. Schematic of the spherical heaving point absorber with a bottom-founded linear PM generator (Tan et al., 2022b).

years, and both its hydrodynamic and electrical characteristics have been well demonstrated (Giorgi et al., 2016; Polinder et al., 2004; Tokat, 2018). Thus, it can be expected to be a representative reference to verify the proposed model.

Fig. 1 depicts the schematic of the studied WEC concept, in which a floating buoy is connected to a bottom-founded PTO system. The floating buoy is defined as the spherical geometry and the diameter is set as 5 m. Besides, the floater is semi-submerged in still water, which implies that the density of the buoy is equal to half of the water. Excited by incoming ocean waves, the floater moves up and down, thus wave power is absorbed as mechanical power.

To convert the absorbed mechanical power to usable electrical power, a linear PM generator is applied as the PTO system in the WEC concept. The translator of the generator is directly linked to the buoy through a rigid connection. In the generator, two identical machines are placed symmetrically to balance the force of attraction. The electronic inverter connected to the output side of the machine is considered as a three-phase back-to-back converter (Polinder et al., 2004). The design of this generator refers to the electrical machine in the AWS wave energy converter (Prado and Polinder, 2013). However, it is scaled down from the original reference machine to fit the size of the floater used in the present paper. The scaling is implemented based on the principle that the force density per area of the active surface of the electrical machines remains identical. More details about the scaling of electrical machines can be found in Tan et al. (2021b). As the translator length, the force limit and the stator current limit of the generator could affect the nonlinearities concerned in this work, their parameters are adjusted in a few simulation cases for identifying the relevance to the accuracy of the proposed model. Hereafter, unless additionally specified, the machine parameters are considered as depicted in Table 1.

Table 1
Specification of the sized generator.

Parameters	Symbol	Quantities
Maximum average power	P_{rated}	220 kW
Maximum force	F_m	100 kN
Maximum velocity	u_{max}	2.2 m/s
Stroke	S	5.0 m
Translator length	L_{tra}	3.0 m
Stator length	L_{sta}	2.3 m
Stack length	l_s	0.46 m
Air gap length	g	5 mm
Slot width	b_s	15 m
Magnet pole width	b_p	79 mm
Tooth width	b_t	18.3 mm
Pole pitch	τ_p	100 mm
Slot pitch	τ_s	33.3 mm
Stator yoke height	h_{sy}	50 mm
Slot height	h_s	85 mm
Magnet thickness	l_m	15 mm
Recoil permeability of the magnets	μ_{rm}	1.1
Remanent flux density of the magnets	B_{rm}	1.1 T at 85 °C
Iron loss per unit mass	P_{Fe0}	4.9 W/kg at 50 Hz and 1.5 T
Copper resistivity	ρ_{Cu}	0.0252 μΩ m at 120 °C
Copper fill factor	k_{sfil}	0.6
Number of conductors per slot	N_s	6
Number of slots per pole per phase	N_p	1

3. Methodology

In this section, the conventional TD approach for constructing the wave-to-wire model is first presented. Next, the derivation of existing SD modeling is extended to cover the wave-to-wire responses. Finally, the set-up of the numerical simulation implemented in this work is detailed.

3.1. Time-domain approach

3.1.1. Representation of incoming waves

The incoming waves are represented based on linear wave theory (Falnes, 2003), and unidirectional waves are considered in this work. The regular wave input is defined as

$$\eta_{re}(t) = \zeta_a \cos(kx - \omega t) \tag{1}$$

where t is the time, k is the wave number, ω is the angular frequency of the incoming wave, and ζ_a is the wave amplitude. Based on the superposition, irregular waves are expressed as

$$\eta_{irr}(t) = \sum_{j=1}^{N} \zeta_a(\omega_j) \cos\left(k(\omega_j)x - \omega_j t + \varphi(\omega_j)\right) \tag{2}$$

where $k(\omega_j)$, $\zeta_a(\omega_j)$ and $\varphi_{(\omega_j)}$ are the wave number, wave amplitude and phase of the regular wave component corresponding to ω_j. Although the Jonswap spectrum is applied in this work, the expression (2) is applicable for various types of wave spectrum (Journée et al., 2015).

3.1.2. Hydrodynamic modeling

The interaction between the buoy and incoming waves is described by hydrodynamic modeling. The buoy is constrained to move in a heaving direction, and only this degree of freedom is discussed. Assuming small WEC motion and limited wave steepness, the linear potential flow theory can be used to solve wave-structure interaction problems in offshore engineering (Folley et al., 2019). In the theory, fluid is assumed to be inviscid, irrotational and incompressible, and thus vortexes and viscosity are neglected. Based on the linear potential flow theory, Cummins equation has been derived and widely applied to describe the motion of a floating buoy subject to ocean waves (Cummins et al., 1962). By adding correction terms, it is possible to extend Cummins equation to allow for the approximation of some transient nonlinear forces, such as drag force and external machinery forces (Folley et al., 2019; Folley, 2016b). In the context of WECs, Cummins equation is commonly represented as

$$\left[M+M_r(\infty)\right]a(t) = F_e(t)+F_{pto}(t)+F_{hs}(t)+F_{vis}(t)+\int_{-\infty}^{t} K_{rad}(t-\tau)u(\tau)d\tau \quad (3)$$

in which M is the mass of the oscillating body, F_e is the excitation force, F_{hs} is the hydrostatic force, K_{rad} is the radiation impulse function, F_{pto} is the PTO force (or generator force); u and a are the velocity and acceleration of the buoy, and F_{vis} is the viscous drag force. $M_r(\infty)$ and K_{rad} represent the added mass evaluated at the infinite frequency and the radiation impulse function. They are calculated based on the results of hydrodynamic damping $R_r(\omega)$ and added mass $M_r(\omega)$. To improve the computational efficiency, the convolution integral of the radiation force is approximated by a state-space representation (Pérez and Fossen, 2008).

According to Silva et al. (2020), the viscous drag force can be estimated by a quadratic damping force, expressed as

$$F_{vis} = -\frac{1}{2}\rho C_D A_D |u(t)|u(t) \quad (4)$$

where ρ is the water density, C_D is the drag coefficient and A_D is the characteristic area of the buoy perpendicular to the moving direction. The drag coefficient is defined as 0.6 based on the study presented in Giorgi and Ringwood (2017a), in which the research geometry was the same as that in the present work. It has to be noted that the quadratic damping term is only an approximation, which is used as a correction term to represent the viscous effects unaddressed in the linear potential flow theory. Morison's equation exemplifies that the physical meaning of the quadratic term can be related to the loss of kinetic energy resulting from factors such as a turbulent boundary layer or larger structures such as vortices (Folley and Whittaker, 2010). As a commonly used approach in the hydrodynamic modeling of WECs, the quadratic damping term with the properly identified drag coefficients has been proven to be an effective and reasonable approximation (Giorgi and Ringwood, 2017b).

In reality, the maximum force that the electrical generator could sustain is limited by its designed capacity. Thus the generator force would be saturated once it is about to violate the limit. In the present study, a passive damping control strategy is implemented in the PTO system (Wilson et al., 2016). This implies that the generator force is proportional to the buoy velocity. Taking the force saturation into account, the generator force can be further expressed as

$$F_{pto}(t) = \begin{cases} -R_{pto}u(t), & \text{for} \quad |R_{pto}u(t)| \le F_m \\ \text{sign}[-R_{pto}u(t)]F_m, & \text{for} \quad |R_{pto}u(t)| > F_m \end{cases} \quad (5)$$

where F_m embodies the PTO force limit.

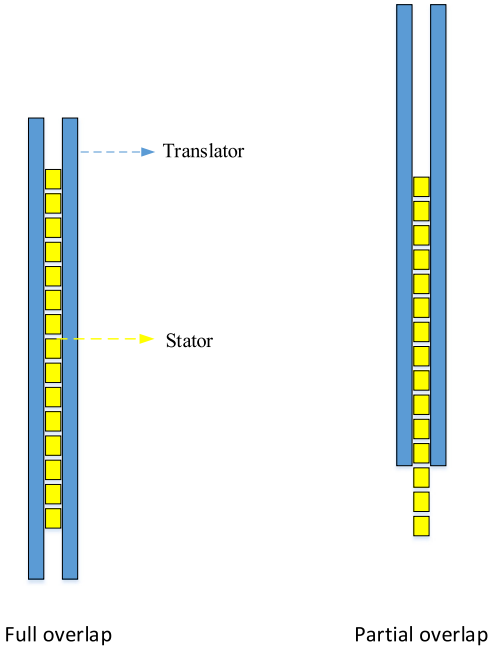

Fig. 2. The schematic of the partial overlap between the translator and stator in a linear generator.

3.1.3. Generator modeling

In this work, an analytical electrical model is applied to calculate the performance of the linear generator. The linear generator converts the absorbed mechanical energy to usable electricity. The design parameters of the generator are shown in Table 1. According to Polinder et al. (2004), generator responses to the buoy movement can be described by an analytical model. As the buoy motion results in the relative movement between the translator and stator of the machine, the no-load voltage is induced and can be calculated as

$$E_p(t) = \sqrt{2}N_m u(t) p l_s N_s k_w |\hat{B}_{gm}| K_{par}(t) \quad (6)$$

where B_{gm} is the fundamental space harmonic of the magnetic flux density in the air gap resulting from the magnets (Polinder et al., 2004), p is the number of pole pairs, l_s is the stack length, N_s is the number of conductors per slot, and k_w is the winding factor. N_m is the machine number, which is set as 2 since the considered linear generator is double-sided. K_{par} is defined as the partial overlap factor, expressed as

$$K_{par} = \frac{l_{act}}{L_{sta}} \quad (7)$$

where l_{act} is the actual length of the overlap between the stator and translator, L_{sta} is the stator length. l_{act} is related to translator displacement, and it can be calculated as

$$l_{act}(z) = \begin{cases} L_{sta}, & \text{for} \quad |z| < 0.5(L_{tra} - L_{sta}) \\ 0, & \text{for} \quad |z| > 0.5(L_{tra} + L_{sta}) \\ 0.5(L_{tra} + L_{sta}) - |z|, & \text{else} \end{cases} \quad (8)$$

where z denotes the displacement of the buoy.

The partial overlap is a particular nonlinear effect occurring in linear generators. It mainly results from the fact the translator length is normally designed to be slightly longer than the stator length for a compromise between the cost and the machine's performance. Fig. 2 presents a schematic of the partial overlap effect when the displacement of the translator is relatively large. The partial overlap has a negative influence on the generator efficiency because a part of the material of

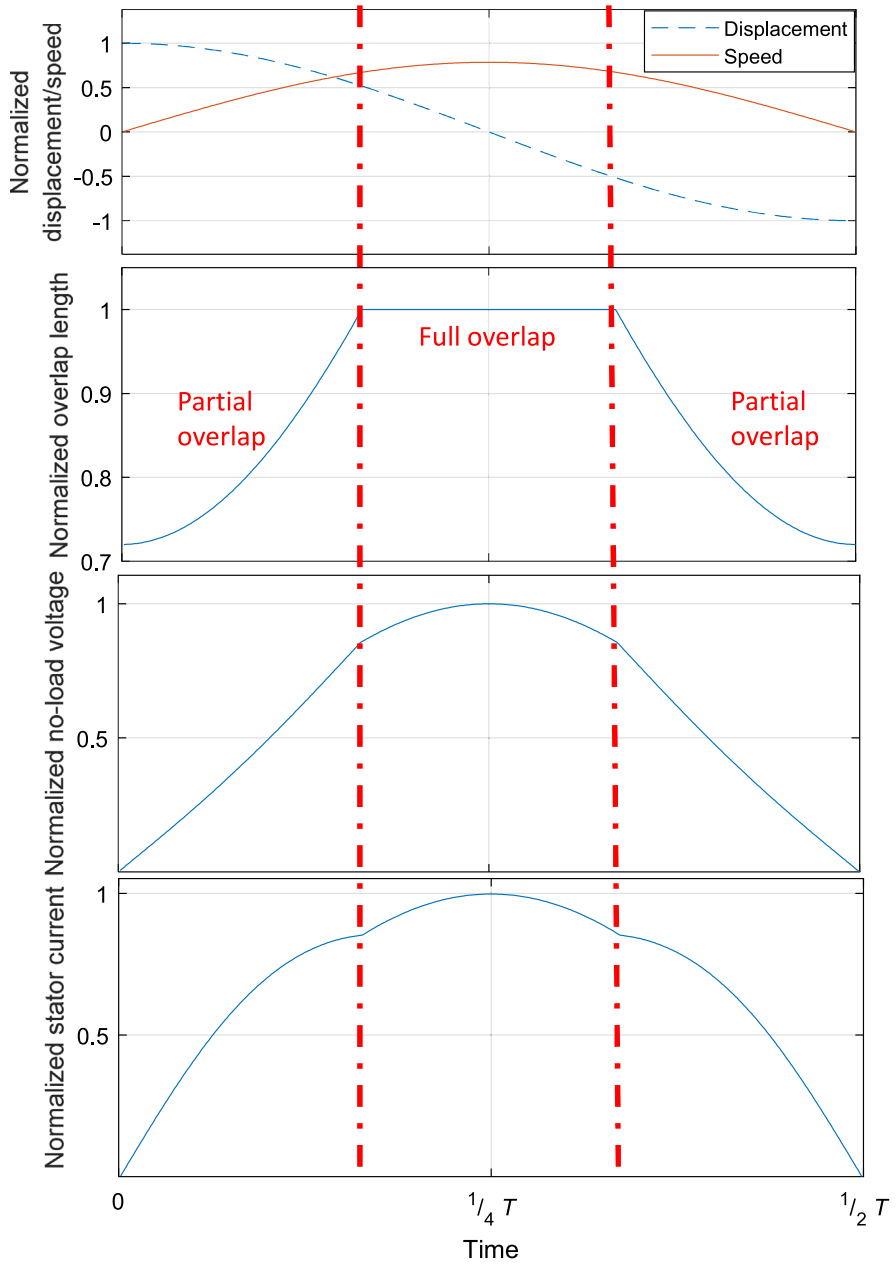

Fig. 3. An illustration of the partial overlap effect on the performance of a linear generator, in which "T" indicates the period of a harmonic oscillation.

the stator is not induced by the magnets mounted on the translator. It leads to the decrease of the total induced no-load voltage, and correspondingly the stator current has to be improved for supplying the required generator force. Fig. 3 shows a good example of the partial overlap effect on the profile of the no-load voltage and stator current when the WEC is excited by a harmonic wave.

The iron losses are dependent on the generator frequency, which can be calculated as

$$P_{Fes} = P_{Fe0}\left[M_{Fest}\left(\frac{\hat{B}_{st}}{B_0}\right)^2 + M_{Fesy}\left(\frac{\hat{B}_{sy}}{B_0}\right)^2\right]\frac{f_e}{f_0}K_{par} \tag{9}$$

where P_{Fe0} is the iron loss per unit mass at the frequency f_0 and flux density B_0; M_{Fest} and M_{Fesy} are the mass of the stator teeth and the stator yoke respectively; f_e is the electrical generator frequency which is dependent on the buoy velocity, and $\hat{B}_{st}$ and $\hat{B}_{sy}$ embody the fundamental space harmonic of magnetic flux density in the stator teeth and yoke. $\hat{B}_{st}$ and $\hat{B}_{sy}$ can be calculated as

$$\hat{B}_{st} = \hat{B}_{gm}\frac{\tau_s}{b_t} \tag{10}$$

$$\hat{B}_{sy} = \hat{B}_{gm}\frac{\tau_p}{\pi h_{sy}} \tag{11}$$

where τ_s and τ_p are the slot pitch and pole pitch; b_t and h_{sy} are the tooth width and stator yoke height. The generator frequency is calculated as

$$f_e(t) = \frac{2\pi|u(t)|}{2\tau_p} \tag{12}$$

The power taken by the generator winding is expressed as the balance of absorbed mechanical power from iron losses, and it is expressed as

$$P_{wd} = F_{pto}(t)u(t) - P_{Fes} \tag{13}$$

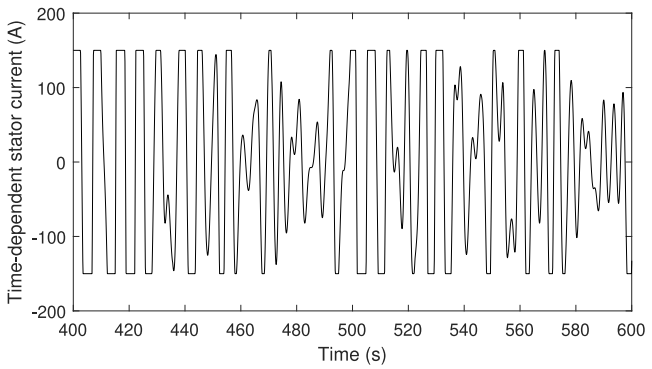

Fig. 4. The profile of the time-dependent stator current of the generator with a current limit, with $H_s = 2.5$ m, $T_p = 7.5$ s and $B_{pto} = 60$ kN s/m.

During operation, the iron losses are negligible compared with the absorbed power (Tan et al., 2022b). Besides, in order to achieve higher system efficiency, the stator current I_s is regulated to be in phase with the no-load voltage E_p (Polinder et al., 2004). Therefore, (13) can be updated as

$$P_{wd} \approx F_{pto}(t)u(t) = mE_p(t)I_s(t) \tag{14}$$

where m represents the phase number of the electrical machine, and it is 3 in this case. It can be deduced from (14) that the linkage between the generator modeling and hydrodynamic modeling is built based on the balance between the power taken by the winding and the absorbed mechanical power. Substituting (6) to (14) gives the expression of the stator current:

$$I_s(t) = \frac{F_{pto}(t)}{m\sqrt{2}N_m p l_s N_s k_w |\hat{B}_{gm}| K_{par}(t)} \tag{15}$$

In electrical machines, another typical nonlinear effect results from the electronic components, namely the stator current limit I_{limit}. When the stator current is about to violate the current limit, the stator current would be saturated. The constraint of the stator current is normally applied to prevent the generator from being overheated. Fig. 4 depicts the time-dependent profiles of the stator current of the considered WEC under a current limit of 150 A, subjected to irregular waves as the input. It is visible that the current limit clearly results in the occurrence of the saturation of the stator current. It is expected to make a difference to the delivered grid power and the overall performance of the system. Therefore, it is of significance to take into account this effect.

It can be noted from (15) that the stator current is directly related to the PTO force. As a consequence, the PTO force saturation is inherently caused by the current limit, and the effect of the current limit is equivalent to that of the PTO force limit in hydrodynamic modeling. Thus, it is not necessary to implement the constraint of the stator current in generator modeling again. For a certain electrical machine, the force limit F_m is correlated with the stator current limit I_{limit} as

$$F_m = m\sqrt{2}N_m p l_s N_s k_w |\hat{B}_{gm}| I_{limit} \tag{16}$$

After the current I_s is derived, the copper losses can be calculated as

$$P_{copper}(t) = mI_s^2(t)R_t \tag{17}$$

where R_t is the stator phase resistance. For simplification, the converter losses P_{conv} are assumed to be only related to the generator side in this model, which can be expressed as

$$P_{conv} = \frac{P_{convm}}{31}\left[1 + 20\frac{|I_s(t)|}{I_{sm}} + 10\left(\frac{I_s(t)}{I_{sm}}\right)^2\right] \tag{18}$$

where P_{convm} is the power dissipation in the converter at the rated operating point, and it is assumed to be 3% of the converter's rated power (Polinder et al., 2006); I_{sm} is rated current of the converter. In (18), the first term is a small constant part standing for the power dissipated in power supplies, gate drivers, control, and cooling system; the second term accounts for the major part that is proportional to the current, and this part is mainly related to the switching losses and conduction losses; the third term is proportional to the current squared, which corresponds to the conduction losses (Polinder et al., 2006).

As the electrical losses have been derived, the electrical power delivered to the grid can be expressed as

$$P_{grid}(t) = P_{wd}(t) - P_{copper}(t) - P_{Fes}(t) - P_{conv}(t) \tag{19}$$

3.2. Spectral-domain approach

SD models are established based on the framework of FD modeling. In SD modeling, nonlinear effects are represented by equivalent linear coefficients in the equations of motion. The equivalent linear coefficients are derived based on stochastic linearization. The existing SD models in literature were only established to predict the hydrodynamic responses of WECs (Silva et al., 2020; Silva, 2019; Folley and Whittaker, 2010, 2013). Thus, in this subsection, SD modeling is first extended to cover the responses of electrical machines. Next, the common nonlinear effects resulting from the electrical generator are linearized and included in the SD model. The derived model enables the calculation of the whole wave-to-wire responses in a pure SD approach. A diagram is shown in Fig. 5 to visualize the structure and solving process of the proposed SD wave-to-wire model.

A key assumption in this SD model is that ocean waves follow the Gaussian distribution. In the context of linear wave theory, the wave elevation is widely thought to be Gaussian distributed, like a wide number of other processes in nature. The reasonableness of the applicability of this distribution can be theoretically supported by the Central Limit Theorem (Bárány and Vu, 2007). The Gaussian process is the most fundamental representation used to describe the stochastic behavior of ocean waves (Journée et al., 2015). The application of the Gaussian process considers that the ocean wave elevation is a sum of a large number of harmonic components which are uncorrelated.

Another assumption is that the WEC system also follows the Gaussian distribution. As demonstrated in Folley (2016b), if a linear system is excited by random Gaussian inputs, the system responses also appear to be Gaussian distributed. It is realized that the incorporation of nonlinear effects into the SD model would challenge the validity of the WEC being a linear system. However, as the SD model is mainly used to estimate the WEC performance in operation wave states instead of extreme conditions, the contributions of nonlinear effects are not expected to be significant. Considering this, it is fair to assume that the WEC system is rather linear and follows the Gaussian process in a good manner.

3.2.1. Hydrodynamic modeling

According to Newton's second law, the motion of the WEC as a rigid body in FD can be described as

$$\hat{F}_e(\omega) = [R_r(\omega) + R_{pto,eq} + R_{vis,eq}]\hat{u}(\omega) + \mathrm{i}\omega\hat{u}(\omega)[M + M_r(\omega)] + \mathrm{i}\hat{u}(\omega)(-\frac{K_{hs}}{\omega}) \tag{20}$$

where $R_r(\omega)$ is the hydrodynamic damping coefficient, R_{pto} is the PTO damping coefficient, ω is the angular wave frequency, $M_r(\omega)$ is the added mass of the buoy, $\hat{u}$ is complex amplitude of the vertical velocity, K_{hs} is the hydrostatic stiffness, and $R_{pto,eq}$ and $R_{vis,eq}$ represent the equivalent linear coefficients for the PTO force saturation and viscous force. Then, by solving (20), the complex amplitude of velocity $\hat{u}$ could be obtained as

$$\hat{u}(\omega) = \frac{\hat{F}_e(\omega)}{R_r(\omega) + +R_{pto,eq} + R_{vis,eq} + \mathrm{i}\omega[M + M_r(\omega)] - \mathrm{i}\frac{K_{hs}}{\omega}} \tag{21}$$

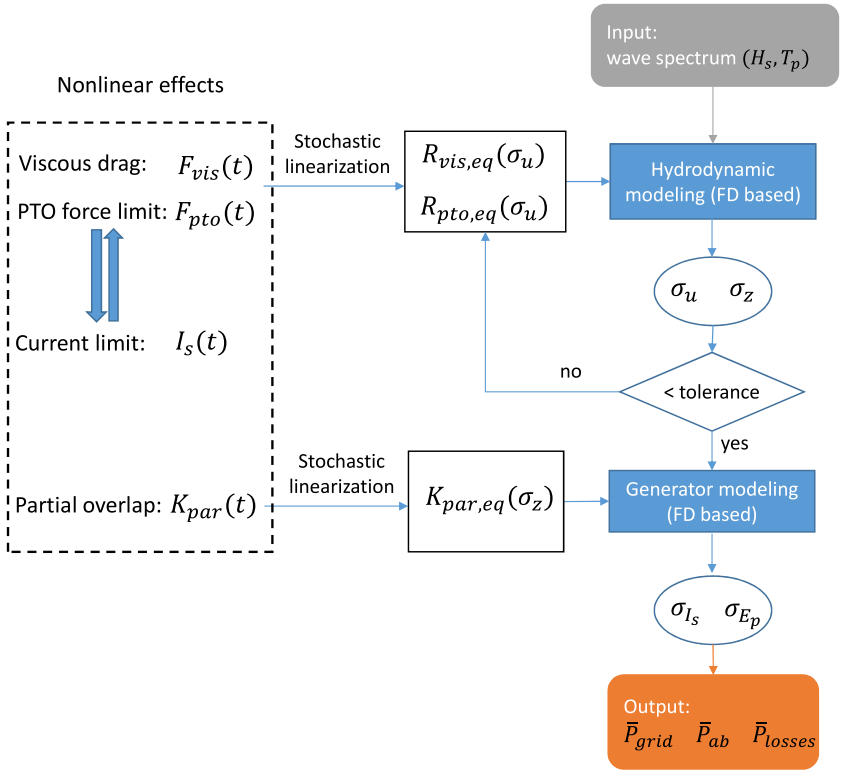

Fig. 5. Diagram of the proposed SD wave-to-wire modeling.

In a predefined wave spectrum, the amplitude of the wave component is related to the wave energy spectrum S_{ζ_a}, as

$$\zeta_a(\omega_j) = \sqrt{2S_{\zeta_a}(\omega_j)\Delta\omega} \tag{22}$$

The variance of the wave elevation $\sigma^2_{\zeta a}$ is calculated as

$$\sigma^2_{\zeta a} = \sum_{j=1}^{N} S_{\zeta_a}(\omega_j)\Delta\omega \tag{23}$$

where $\sigma_{\zeta a}$ is the standard deviation of the wave elevation. Similarly, as the velocity amplitude of WEC corresponding to each wave component can be obtained by (21), the standard deviation and spectral density of the WEC response can be calculated. Then, the mean absorbed power can be derived as

$$\overline{P}_{ab} = \sum_{j=1}^{N} \frac{1}{2} R_{pto,eq} \left|\hat{u}(\omega_j)\right|^2 = \sum_{j=1}^{N} R_{pto,eq} S_u(\omega_j)\Delta\omega = R_{pto,eq}\sigma_u^2 \tag{24}$$

where S_u and σ_u denote the spectral density and standard deviation of the velocity of the WEC.

3.2.2. Generator modeling

The hydrodynamic model presented above can be used to predict the mechanical power absorbed by the buoy, but the electrical power could not be reflected. The conversion from the absorbed power to the delivered electrical power is associated with electrical responses. Given the random phase assumption of wave input to the WEC system, it is possible to describe the generator responses in SD.

Based on (6), the complex amplitude of the no-load voltage in each frequency component is expressed as

$$\hat{E}_p(\omega) = \sqrt{2} N_m \hat{u}(\omega) p l_s N_s k_w |\hat{B}_{gm}| L_{sta} K_{par,eq} \tag{25}$$

where $K_{par,eq}$ is the equivalent linear coefficient of the time-dependent partial overlap coefficient K_{par}. The linearization will be detailed in the following text.

The power taken by the generator winding, namely P_{wd}, at each frequency component is calculated as

$$P_{wd}(\omega) = \frac{1}{2}\mathrm{Re}\{\hat{F}_{pto}(\omega)\hat{u}^*(\omega)\} = \frac{1}{2}|\hat{F}_{pto}(\omega)||\hat{u}(\omega)| = \frac{1}{2} R_{pto,eq}|\hat{u}(\omega)|^2 \tag{26}$$

Thus, the magnitude of the complex amplitude of the stator current at each frequency component can be calculated as

$$|\hat{I}_s(\omega)| = \frac{R_{pto,eq}|\hat{u}(\omega)|^2}{m|\hat{E}_p(\omega)|} \tag{27}$$

As the effect of the PTO force limit has been incorporated by the equivalent linear coefficient $R_{pto,eq}$, the current limit is therefore taking effect correspondingly. Then, the standard deviation of the stator current is derived as

$$\sigma_{I_s} = \sqrt{\frac{1}{2}\sum_{j=1}^{N} |I_s(\omega_j)|^2} \tag{28}$$

At this point, the relevant hydrodynamic and electrical responses can be estimated in statistical form based on the SD modeling presented above. To further reveal the generator performance, the electrical losses have to be derived in the statistical form corresponding to the expressions in the TD approach. The copper losses of the generator are calculated as

$$\begin{aligned}\overline{P}_{copper} &= \langle m I_s^2 R_t \rangle \\ &= m R_t \sigma^2_{I_s}\end{aligned} \tag{29}$$

Assuming that the variable I_s follows the Gaussian distribution, it gives

$$\langle |I_s| \rangle = \sqrt{\frac{2}{\pi}}\sigma_{I_s} \tag{30}$$

This enables the prediction of the converter losses, expressed as

$$\overline{P}_{conv} = \frac{1}{31}P_{convm} + \frac{20}{31I_{sm}}P_{convm}\langle|I_s|\rangle + \frac{10}{31I_{sm}^2}P_{convm}\langle I_s^2\rangle$$
$$= \frac{1}{31}P_{convm} + \frac{20}{31I_{sm}}P_{convm}\sqrt{\frac{2}{\pi}}\sigma_{I_s} + \frac{10}{31I_{sm}^2}P_{convm}\sigma_{I_s}^2 \tag{31}$$

The iron losses are calculated as

$$\overline{P}_{Fes} = P_{Fe0}\left[m_{Fest}\left(\frac{\hat{B}_{st}}{B_0}\right)^2 + m_{Fesy}\left(\frac{\hat{B}_{sy}}{B_0}\right)^2\right]\frac{\langle f_e\rangle}{f_0}K_{par,eq} \tag{32}$$

where $\langle f_e\rangle$ can be related to the standard deviation of the absolute value of the buoy velocity, and assuming the Gaussian assumption of the response gives

$$\langle f_e\rangle = \frac{2\pi}{2\tau_p}\langle|u|\rangle$$
$$= \frac{\pi}{\tau_p}\sqrt{\frac{2}{\pi}}\sigma_u \tag{33}$$

Therefore, the mean grid power can be derived as

$$\overline{P}_{grid} = \overline{P}_{wd} - \overline{P}_{copper} - \overline{P}_{Fes} - \overline{P}_{conv} \tag{34}$$

3.2.3. Stochastic linearization

The method to implement stochastic linearization of the relevant nonlinear effects in the hydrodynamic stage has been demonstrated in previous Refs. Silva et al. (2020), Tan et al. (2022a) and Folley and Whittaker (2010). Thus, the derivation of equivalent linear coefficients is only briefly discussed here for nonlinearities related to the hydrodynamic responses. The equivalent linear coefficients $R_{pto,eq}$ and $R_{vis,eq}$ representing the effect of the PTO force saturation and viscous force are considered in the hydrodynamic stage. The principle of linearization is to balance the expected value of the dissipated power and the power dissipated by an equivalent linear term. According to Folley and Whittaker (2010), the equivalent coefficient of a generic nonlinear force F_{non} in the hydrodynamic modeling can be calculated as

$$R_{eq} = \langle\frac{\partial F_{non}(u)}{\partial u}\rangle$$
$$= \int_{-\infty}^{\infty}\frac{\partial F_{non}(u)}{\partial u}p(u)\mathrm{d}u \tag{35}$$

where F_{non} embodies the concerned nonlinear force, and $p(u)$ is the probability density function of the response u. Assuming the Gaussian process of the response, the probability density function is expressed as

$$p(u) = \frac{1}{\sigma_u\sqrt{2\pi}}\exp(-\frac{u^2}{2\sigma_u^2}) \tag{36}$$

As demonstrated above, a particular nonlinear effect in linear generators results from the partial overlap between the stator and translator of the machine. The generic expression of the power dissipated by a load in an electrical circuit can be expressed as

$$P_{dis}(t) = \left[\frac{I_s(t)}{K_{par}(t)}\right]^2 R_t \tag{37}$$

Given random inputs, its expected value can be calculated as

$$\langle P_{dis}\rangle = \langle I_s^2\rangle\langle\frac{1}{K_{par}^2}\rangle R_t \tag{38}$$

It can be deduced that K_{par} is non-negative, thus (38) can be rewritten as

$$\langle P_{dis}\rangle = \sigma_{I_s}^2\frac{1}{\langle K_{par}^2\rangle}R_t \tag{39}$$

As K_{par} is an even function with regard to the variable z, the equivalent linear coefficient $K_{eq,par}$ can be derived as

$$K_{par,eq} = \sqrt{\langle K_{par}^2\rangle}$$
$$= \sqrt{2\int_0^{\infty}K_{par}^2(z)p(z)\mathrm{d}z} \tag{40}$$

where $p(z)$ is the probability density function of the displacement of the buoy, and it is expressed as (36) with the Gaussian assumption. It can be noticed that the iteration process is not needed for obtaining $K_{par,eq}$. This is because it is dependent on the standard deviation of the buoy displacement z which could be explicitly derived from the hydrodynamic modeling and takes effect as the input to generator modeling.

The stochastic linearization in the SD model is carried out based on the assumption that the WEC system follows the Gaussian process. It has to be acknowledged that the addition of nonlinear effects contradicts this assumption. As the nonlinear effects become stronger, the Gaussian assumption becomes less valid. Therefore, it can be expected that the linearized representations would be less effective when the intensity of the considered nonlinear effects increases. As a consequence, the SD model tends to be less accurate in the circumstances.

3.3. Simulation implementation

The simulation set-up is presented in this subsection. In this work, irregular waves are represented based on the superposition of 500 individual harmonic wave components. The angular frequencies of the wave components are uniformly spaced from 0.05π to 4π rad/s. The random phase assumption is applied to the wave components, and the JONSWAP spectrum with a peakedness factor of 3.3 is considered for the irregular wave states.

The hydrodynamic coefficients of the floater, namely $M_r(\omega)$, $R_i(\omega)$ and $f_e(\omega)$, are numerically derived based on the Boundary Element Method using the open source software Nemoh (Penalba et al., 2017b). With respect to TD modeling, direct calculation of the convolution integral of the radiation force in (21) requires huge computational efforts. In this work, it is replaced by a state-space approximation for saving simulation time. The state-space parameters are derived by the frequency-domain identification method as proposed in Pérez and Fossen (2008). The partial differential equations in TD modeling are solved by a numerical integration scheme based on the ODE 45 solver in the commercial MATLAB environment. The initial displacement and velocity of the floater are set to zero. The simulation time duration and time step are set to 200 times and 0.01 times the considered peak period T_p respectively. A ramp function is used to avoid strong transient flow at first time steps, and the ramp time is chosen as 25 T_p (Lawson et al., 2014). The duration of the ramp time is not included in the analysis of the power performance of WECs. As the random phase assumption is associated with random errors in the results, each case in TD simulation is re-run 10 times for deriving the mean values. In the SD simulation, as the iterative process is required to solve the standard deviation of the buoy velocity, a convergence tolerance of 0.1% is defined in the iterative process of solving the standard deviation of the responses (Silva et al., 2020; Folley and Whittaker, 2013).

4. Results and discussion

The simulation results obtained by the established SD wave-to-wire model are presented in this section, and they are verified against those generated by the conventional TD wave-to-wire model. To better demonstrate the relevance of different sources of nonlinearities to the modeling accuracy, the influence of the partial overlap and the stator current constraints is discussed respectively. Finally, The variation of the computational efficiency of the SD model with the tolerance of iterations is identified and compared with TD modeling.

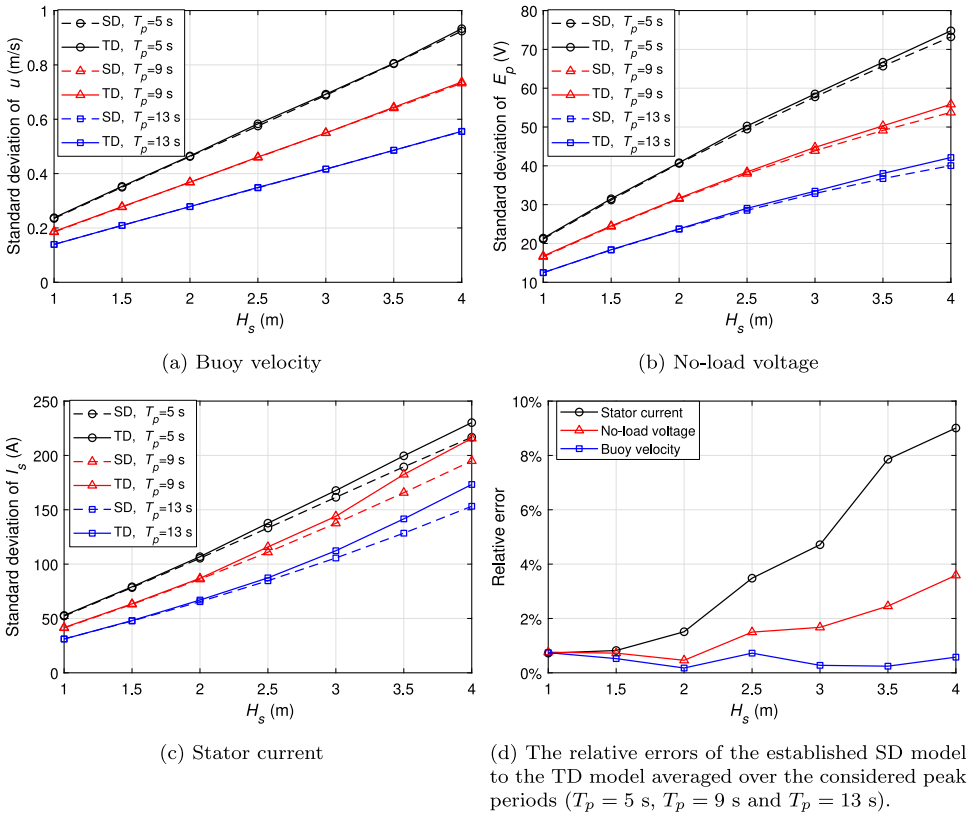

(a) Buoy velocity

(b) No-load voltage

(c) Stator current

(d) The relative errors of the established SD model to the TD model averaged over the considered peak periods ($T_p = 5$ s, $T_p = 9$ s and $T_p = 13$ s).

Fig. 6. The standard deviation of the responses of the WEC in different wave states and the relative errors of the SD model to the TD model. ($B_{pto} = 60$ kN s/m).

4.1. Model verification

A variety of wave states are considered in the simulation cases of verification. The concerned peak periods T_p range from 5 s to 13 s, and the considered significant wave heights H_s are between 1 m to 4 m. In Fig. 6, the standard deviation of the responses, including the buoy velocity, stator current and induced no-load voltage, obtained by the SD model and the TD model are compared. The relative errors of the SD model to the TD model are also identified. It can be seen that the proposed SD model has an adequate agreement with the conventional TD model. The maximum relative errors for the stator current, no-load voltage and floater velocity are 9%, 4% and 1%.

As illustrated in Fig. 6, With the increase of the significant wave height, the accuracy of the proposed SD model tends to decrease. This can be explained by the fact that the increased significant wave height results in a larger buoy motion. The buoy motion is a strong factor in the nonlinearity of the system. For instance, as the buoy motion is larger, the buoy velocity would be higher. It can be inferred from (9) that the increased velocity contributes to the increase of the PTO force. Then, the PTO force constraint could take effect and make a nonlinear contribution to the system. As the nonlinear effects become more dominating, a physical implication to the SD modeling is that the Gaussian assumption would be weakened. Consequently, the equivalent linear terms derived based on the Gaussian assumption would be less effective and take larger errors into the estimation.

Another noteworthy point is that the estimation of generator responses is associated with higher relative errors than those of the hydrodynamic response. As shown in Fig. 6(d), the relative error of the stator current and no-load voltage is clearly larger than that of the buoy velocity in the identical simulation conditions. The reason is that the generator modeling in the proposed SD model relies on the calculated hydrodynamic responses, including the buoy velocity and displacement, as the inputs. Specifically, as explained in the text below (40), the partial overlap factor K_{par} in the generator modeling is linearized based on the explicitly derived standard deviation of the buoy displacement. Hence, this part of sources of error inherently remains in the generator modeling of the SD approach. Furthermore, it can be deduced from the mathematic derivation of the generator responses that the error from the hydrodynamic modeling is even amplified. For instance, as given in (25), the complex amplitude of the no-load voltage is proportional to the product of the complex amplitude of the velocity and the linearized partial overlap factor. Both these two variables are associated with the source of the error from the hydrodynamic part of the SD modeling. This explanation also applies to the derivation of the stator current of the SD modeling, given in (27). In this sense, the relative error of the estimation of the generator responses presents to be relatively more obvious than those of the hydrodynamic responses.

As an extension of the FD approach, it is of importance to verify the accuracy of the SD model in estimating the responses in different frequency components. Thus, the power spectral density of the stator current, the no-load voltage and the buoy displacement are calculated using the TD and SD models respectively, which are depicted in Fig. 7. The SD model presents a reasonable prediction of the responses in a range of frequencies. In addition, it can be observed in Fig. 7(c) that the peak frequency of the buoy displacement is highly aligned with that of the incident wave. Comparing it with Fig. 7(a) and (b), it can be found that the no-load voltage and the stator current also correspond to an identical peak frequency, which is around 0.14 Hz. Besides, in Fig. 7, there does not appear any visible additional harmonic peak in the power spectral density of the WEC responses even though nonlinear effects are taken into account. This is because the SD model is supposed to be applied mainly for operation regions with moderate nonlinear effects. Thus, the considered condition in the figure is defined away from extreme cases. Given this, the point absorber behaves as an inertial-dominating system, where the nonlinear components are not sufficiently intensive to result in a visible second peak in the profile of the power spectral density of the responses (Folley, 2016a).

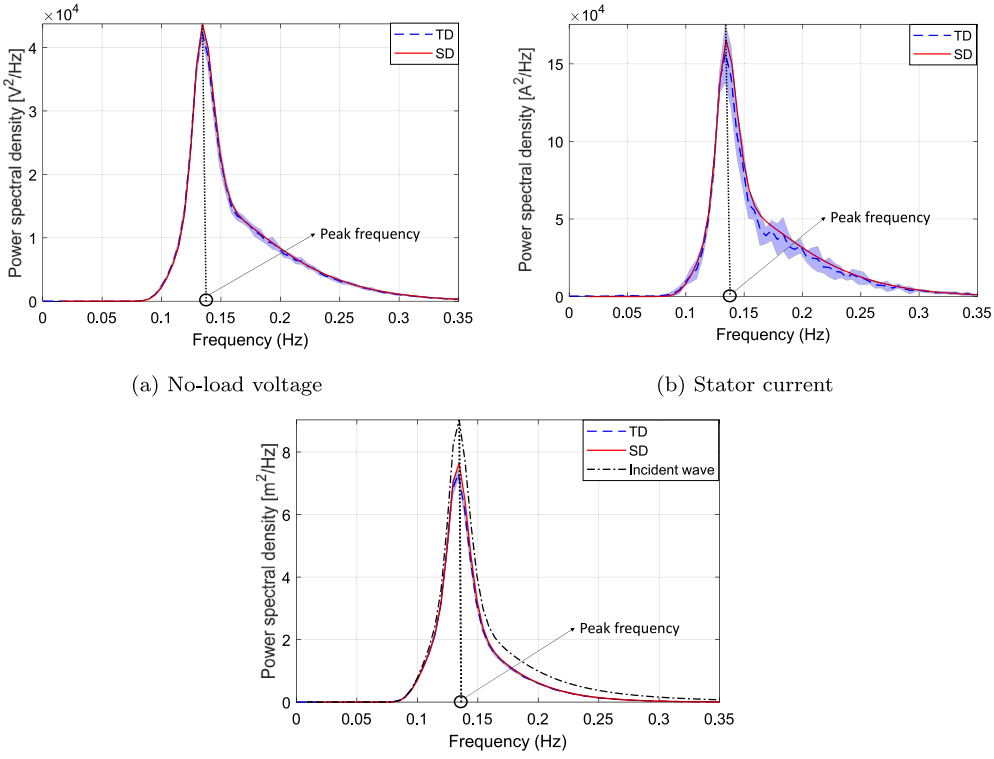

(a) No-load voltage

(b) Stator current

(c) Displacement of the buoy and incident wave elevation

Fig. 7. The power spectral density of the relevant WEC responses and of the incident wave elevation. (B_{pto} = 60 kN s/m, H_s = 2.5 m and T_p = 7.5 s) The shaded area represents the standard deviation of the results of the TD model.

An upside of wave-to-wire modeling is to holistically reveal the power conversion efficiency throughout the complete operation process of the system. To further verify the accuracy of the established SD wave-to-wire model, the absorbed power, grid power, copper losses, converter losses and power conversion efficiencies are calculated and compared with the results from the TD wave-to-wire model. The power conversion efficiency herein is defined as the delivered electrical power to the grid divided by the absorbed mechanical power by the floater. As shown in Fig. 8, the proposed SD model could accurately predict the power and losses in different power conversion stages. The relative error of the SD to the TD model is less than 7% with regard to the estimate of the power conversion efficiency even when the significant wave height is as large as 4 m. For typical operational significant wave heights (below 2.5 m), the relative error is no more than 2%.

4.2. Relevance of the partial overlap effect

The nonlinearities in the hydrodynamic stage, such as viscous drag force, have been thoroughly studied in previous research in terms of SD modeling (Silva et al., 2020; Tan et al., 2022a). Thus, given the purpose of this work, more attention is paid to the effects in the electrical generator. A particular effect addressed in this subsection is the partial overlap between the stator and the translator. To reveal the relevance of the translator length on the intensity of the partial overlap effect and the model accuracy, the translator length is varied in the simulation implementation. The corresponding results are shown in Figs. 9 and 10. Shortening the translator decreases the value of the equivalent linear coefficient representing the partial overlap effect, namely $K_{par,eq}$. For instance, at the peak period of 13 s, it is approximately 0.95 for the ratio between the translator length and stator length is 1.6 while it is reduced to 0.8 for the ratio of 1.1. This is expected since the reduction of the translator length is correlated with the increase in the intensity of the partial overlap effect. Affected by the partial overlap, the values of the no-load voltage decrease, thus the equivalent linear coefficient $K_{par,eq}$ becomes smaller as can be deduced from (25).

Fig. 10 shows the estimated standard deviation of the stator current with different translator lengths of the linear generator. The shorter the translator's length, the more nonlinear the system could be. Therefore, the relative error of the SD model to the TD model becomes larger with the increase of the translator length. However, Fig. 10 also implies that the proposed SD model has a satisfying accuracy for the translator lengths ranging from 1.1 to 1.6 times the stator length. For instance, the relative error is still within 7% when the ratio is reduced to 1.1. However, this is an extreme case since the translator length would hardly be designed to be so close to the length of the stator.

4.3. Relevance of the stator current limit

In this subsection, attention is drawn to the influence of the stator current limit on the accuracy of the established SD model. To mitigate the disturbance of the effect of the partial overlap, the translator length is adjusted to be sufficiently high, namely 4.5 m, in the discussed cases as follows. This is almost twice the length of the stator length, thus the partial overlap effect can be thought minor. In the simulation, various current limits are implemented, and the corresponding results of the TD and SD models are presented and compared.

Fig. 11 depicts the standard deviation of the stator current, in which different significant wave heights are taken into account. It is reasonable to be noted that the standard deviation of the stator current tends to increase with the imposed current limit, which also implies that the defined range of the current limits is representative of studying the relevance of the current limit. In Fig. 12, the power conversion efficiency of the WEC obtained by the SD and TD models is compared. The efficiency generally presents a descending trend with the current limit. This mainly results from the fact that the magnitude of the stator current increases with the current and the higher stator

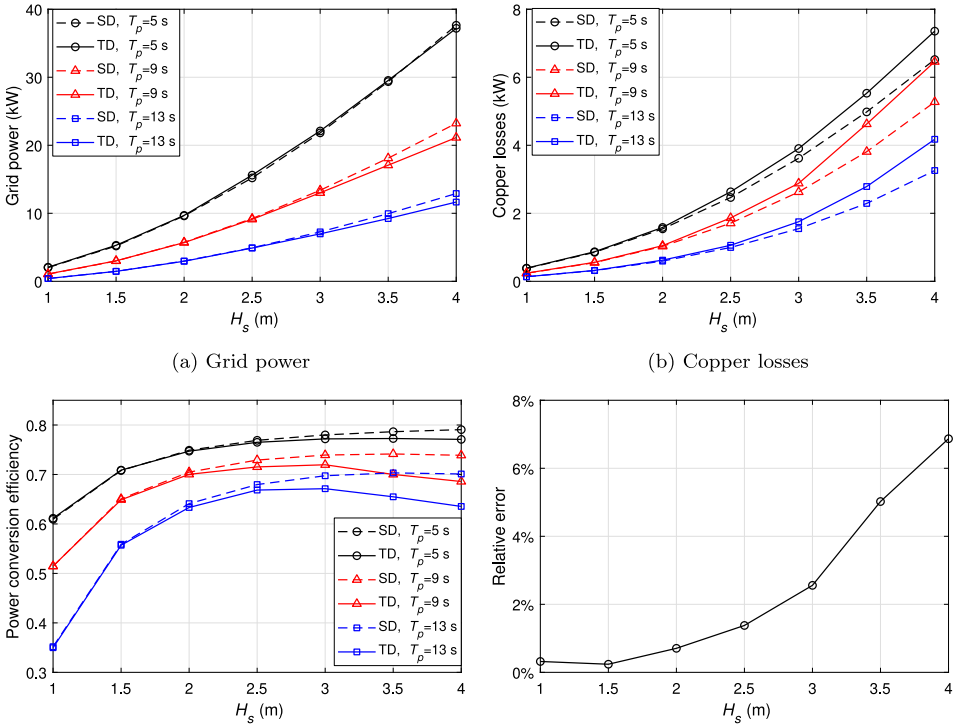

(a) Grid power

(b) Copper losses

(c) Power conversion efficiency

(d) The relative errors of the established SD model to the TD model with regard to the power conversion efficiency, and the values are averaged over the considered peak periods (T_p = 5 s, T_p = 9 s and T_p = 13 s).

Fig. 8. Grid power, copper losses and power conversion efficiency of the WEC in different wave states and the relative errors of the SD model to the TD model. (B_{pto} = 60 kN s/m).

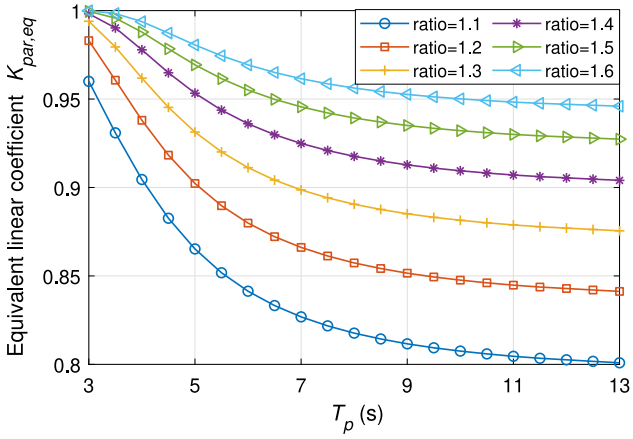

Fig. 9. The derived linear equivalent coefficient for the partial overlap effect $K_{par,eq}$ with different translator lengths. The simulation is implemented in the case with H_s of 3.0 m and B_{pto} of 60 kN s/m. The "ratio" in the legend indicates the ratio between the translator length and stator length, and the stator length is considered constant as 2.3 m.

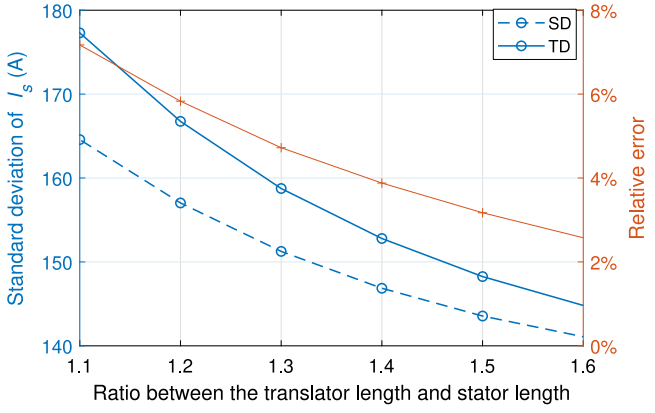

Fig. 10. The standard deviation of the stator current calculated by the SD and TD models with different translator lengths and the relative error of the SD model to the TD model. (H_s = 3.0 m, T_P = 7.5 s and B_{pto} = 60 kN s/m).

current is associated with higher electrical losses. In addition, it is seen in both Figs. 11 and 12 that the discrepancy between the results of the SD and TD models is more noticeable in lower current limits or larger significant wave heights. This is because the stator current is more likely to violate the current limit in these two circumstances and the occurrence of the current being saturated would be more frequent. Then, the Gaussian assumption is more challenged by the increased intensity of the nonlinearities, which leads to the reduction of the modeling accuracy. But even in extreme cases, the established SD model still has a good consensus with those of the TD model. For instance, when the current limit is 130 A and the significant wave height is 3 m, the calculated standard deviation of the stator current and the power conversion efficiency is 98.3 A and 0.818 for the SD model, while they are 103.3 A and 0.792 for the TD model. Accordingly, the relative errors are quantified as 4.8% and 3.2% with regard to the standard deviation of the stator current and power conversion efficiency respectively. Furthermore, the power spectral density of the

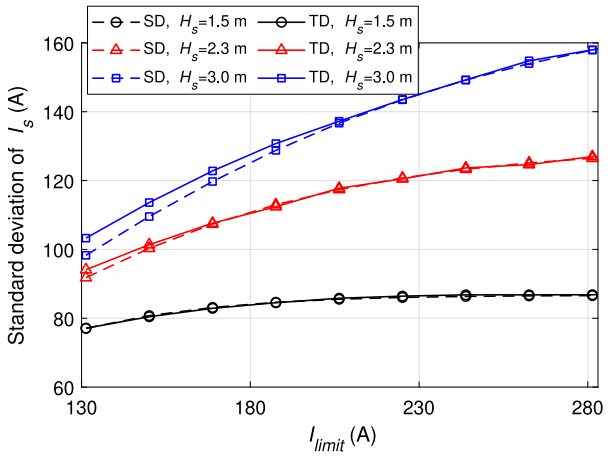

Fig. 11. The standard deviation of the stator current of the generator with different current limits, and with $T_p = 7.5$ s and $B_{pto} = 80$ kN s/m.

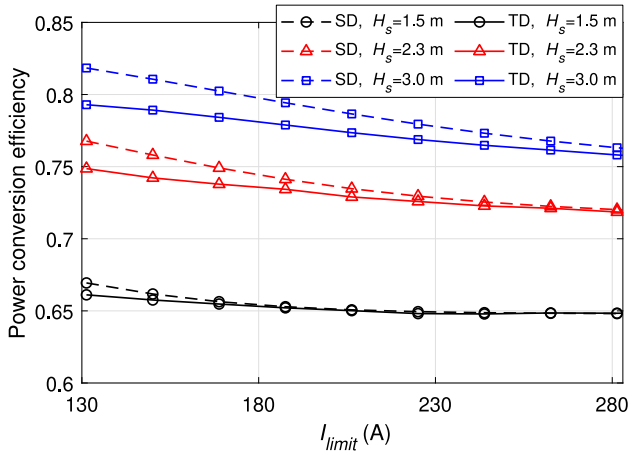

Fig. 12. The power conversion efficiency of the WEC with different current limits, and with $T_p = 7.5$ s and $B_{pto} = 80$ kN s/m.

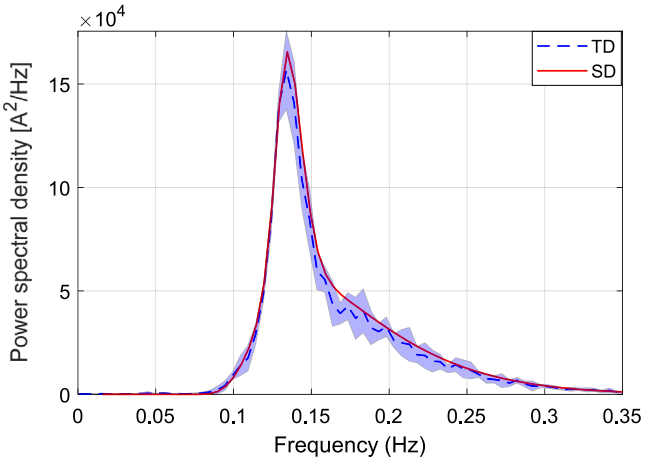

Fig. 13. The power spectral density of the stator current with a current limit of 150 A. ($B_{pto} = 80$ kN s/m, $H_s = 2.5$ m and $T_p = 7.5$ s) The shaded area represents the standard deviation of the results of the TD model.

stator current calculated by the SD and TD model is compared in Fig. 13, which shows a good agreement between them in different frequency components.

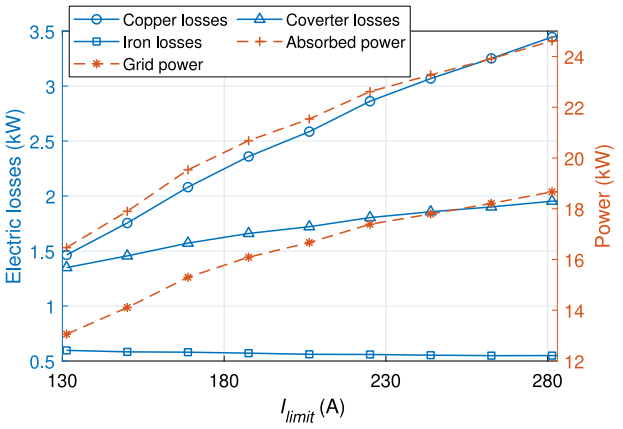

Fig. 14. The power and electric losses of the WEC with different current limits, and with $T_p = 7.5$ s and $B_{pto} = 80$ kN s/m. The results are generated by TD model.

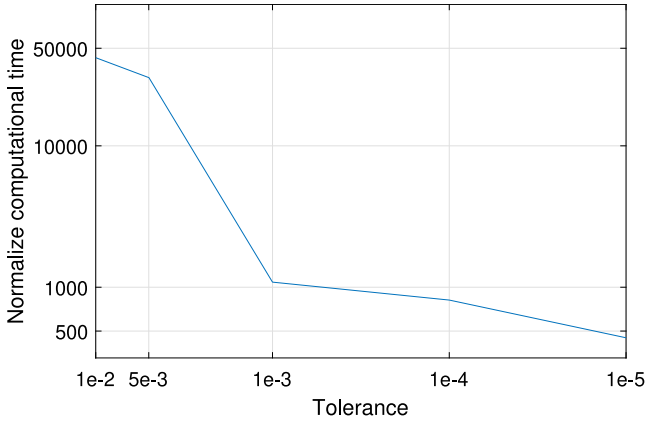

Fig. 15. The normalized computational time of the TD model to the SD model with different tolerances of the iterations in SD modeling.

To demonstrate the relation of the power conversion efficiency to the current limit, the electric losses and power of the WEC corresponding to various current limits are presented in Fig. 14. It is visible that the main sources of electric losses, in this case, can be regarded as the copper losses and converter losses, while the iron losses are negligible. These two main losses increase with the current limit. This can be explained by (17) and (18) as they both present a clear positive correlation with the current squared. Besides, the increase of the current limit leads to the improvement of the absorbed power since the resulted larger PTO force limits inherently imply a higher power capacity of the WEC. However, the increase of the copper losses with the current limit is stronger than that of absorbed power. For instance, at the current limit of 130 A, the value of the copper losses is 1.5 kW and it is around 16 kW for the absorbed power. In this sense, the proportion of the copper losses to the absorbed power is 9.3%. When the current limit is raised to 280 A, the copper losses and the absorbed power are 3.5 kW and 25 kW respectively. The copper losses then account for approximately 14% of the absorbed power. Therefore, it is understood that the power conversion efficiency decreases with the increase of the current limit, as depicted in Fig. 12.

4.4. Computational efficiency

The main motivation for applying SD rather than TD wave-to-wire modeling is to save computational load. Fig. 15 depicts the relation of the normalized computational time to the tolerance of the iterations. All the simulations in this work are performed in an identical machine

which is equipped with an Intel i7/2.80 GHz processor. For the TD modeling, the computational time is counted by a single-run simulation, and the computational time was counted as 7.1 s. However, it is known that multiple simulations are required to mitigate the error resulting from the set of random phases of incoming waves. However, it is seen that the established SD model is still faster than the conventional TD modeling by around five hundred times when the tolerance of iterations in SD modeling is as strict as $1e^{-5}$.

4.5. Discussion

The proposed SD wave-to-wire model demonstrates satisfactory accuracy compared to the conventional TD modeling approach. However, it is essential to acknowledge that the achievements presented in this study are specifically focused on a specific case involving a point absorber with a linear PM generator. One of the major challenges in the field of WECs is the significant divergence among various technologies (Tiron et al., 2015). Different WEC concepts vary considerably in terms of their power capture principles, PTO systems, operational regions, and other aspects. For example, another promising type of WEC is the OWC device (Delmonte et al., 2016). In this case, power capture is based on pressure variations in an air chamber, which then drives a turbine connected to a generator through the airflow (Heath, 2012). The nonlinear characteristics involved in this process are significantly different from those observed in point absorbers. Consequently, the proposed SD model is expected to have limited applicability to OWC devices. To make a more substantial contribution to the advancement of WECs, it is crucial to extend the current SD model to encompass different applications of WECs in the future.

This study performs the verification of the SD model by considering various factors that can influence its accuracy. These factors include different wave conditions, ratios between the translator and stator lengths, and current limits of the linear generator. The variations in these factors can impact the accuracy of the proposed SD model due to their correlation with the nonlinearity of the entire WEC system. It is acknowledged that this observation can be extended to include additional parameters of individual components. For example, the size or shape of the buoy can significantly affect the responses of the WEC, leading to varying levels of nonlinear effects and potentially influencing the accuracy of the SD model. Moreover, the topology and type of the electrical generator, as well as the specifications of the electronic converter, can also contribute to the overall behavior of the system (Tan et al., 2022b; Polinder, 2013; Polinder et al., 2005) and subsequently affect the accuracy of the SD model. Therefore, it is suggested to perform verification when applying this SD wave-to-wire approach to different device parameters or a wider range of wave conditions. By doing so, a better understanding of the model's accuracy can be achieved and potential limitations or areas for improvement can be identified.

The hydrodynamic modeling utilized in this manuscript is based on linear potential flow theory and is described by the Cummins equation (Giorgi, 2017). The Cummins equation and its extension have been widely used to model the behavior of WECs, while it should be realized that it is inherently limited to operation conditions where the nonlinear effects are negligible or moderate (Folley, 2016b). An extended form of the hydrodynamic model is applied in this study, which incorporates the nonlinear drag force and the nonlinear PTO force. This inclusion helps alleviate the restrictions imposed by the linear hydrodynamic model. Nonetheless, it is crucial to recognize that the validity of this hydrodynamic model may still face challenges when dealing with severe wave conditions. In powerful wave states, the motion of the WEC becomes more pronounced. Consequently, other nonlinear forces such as the nonlinear Froude–Krylov force and hydrostatic force are also expected to have an impact (Giorgi and Ringwood, 2017b). Moreover, the increased wave steepness in powerful wave states becomes relevant to wave nonlinearity, potentially violating the assumption of linear potential flow theory. Therefore, it is necessary to determine the appropriate application range of the SD model, keeping in mind that its intended purpose is to model WECs under normal operating conditions.

In this work, the proposed SD model is verified by comparing the results against those generated by the TD modeling. It can be challenged that experimental validation provides a more realistic assessment of the accuracy of the SD model. However, the SD model in principle is not expected to be more accurate than the TD model in describing the physical reality. This is because all the nonlinear effects incorporated in the SD model are linearized based on their expressions in TD modeling. It is known that linearization could improve computational efficiency, but it would inevitably result in reduced accuracy. Thus, the TD model can be thought of as a reference with the desired accuracy with regard to the SD model. When a newly developed SD model is being verified, it can be an economical and efficient approach to compare it with the corresponding TD model, as implemented in other relevant publications (Folley and Whittaker, 2010; Silva et al., 2020). Given these considerations, it is reasonable to utilize TD modeling as a reference for verification purposes.

This study focuses on the concept of a heaving point absorber coupled with a linear PM generator. Point absorber WECs are commonly recognized for their high power absorption efficiency, primarily attributed to their small horizontal dimensions relative to the wavelength, which makes them less sensitive to the wave direction (Falnes and Hals, 2012). The implementation of a direct-drive PTO system using a linear generator has also been acknowledged as an effective solution due to the reduction in intermediate power transmission stages (Polinder, 2013). However, for more realistic applications, the performance of WECs is influenced by various factors. One such factor is the hydrodynamic interaction between multiple WECs, which can impact the power capture efficiency of individual devices. This effect becomes particularly significant when WECs are arranged in the configuration of a closely-located array or farm (Vervaet et al., 2022). It is important to note that this study focuses only on one single point absorber. Thus, extending the current SD model to allow for multiple WECs is expected to make a larger contribution. Furthermore, the availability of wave power exhibits seasonal variability, which might lead to significant fluctuations in the power output of WECs (Carballo and Iglesias, 2012). Consequently, relying solely on mean annual wave characteristics for energy production estimation may result in misleading conclusions. In this sense, the applicability of the proposed SD wave-to-wire model is potentially necessary to be examined for different wave characteristics. In addition, the efficiency of this type of WEC is also dependent on its size, adopted control strategy, the topology of the generator, wave conditions of the site, etc (Tan et al., 2021a, 2020; Tedeschi and Molinas, 2012; Babarit, 2015; Polinder et al., 2005). Considering the aforementioned factors, it is crucial to pay attention to these considerations when employing the SD wave-to-wire modeling technique for assessing the performance of WECs in numerical simulations.

5. Case study: tuning PTO damping coefficients

A case study is carried out in this section to demonstrate the performance of the proposed SD modeling. It is applied to tuning the PTO damping of WECs while FD modeling and TD modeling are used at the same time for comparison. As a control parameter, PTO damping plays an important role in the power performance of WECs. Even though a number of real-time control algorithms have been proposed and applied for WECs in recent years (Wang and Isberg, 2015; Garcia-Rosa et al., 2017; Fusco and Ringwood, 2011; Anderlini et al., 2017). With regard to the early-stage design of WECs, it is significant to search for a constant PTO damping for maximizing the power production in each wave state since it is associated with lower complexity and could also effectively reflect the potential of the device.

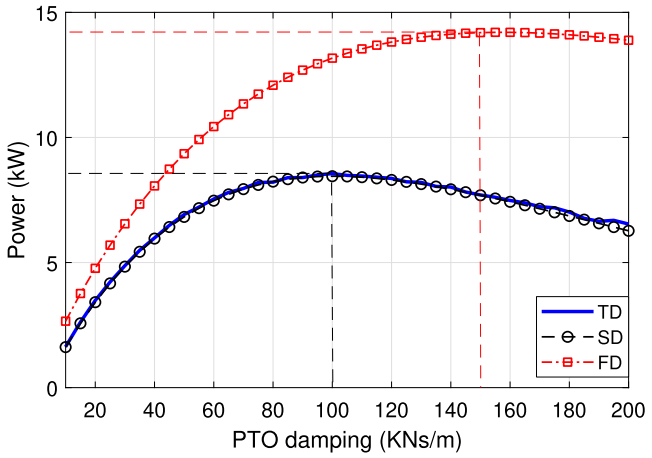

Fig. 16. The power estimate of WECs predicted by three different models with various values of the PTO damping. ($H_s = 2.0$ m and $T_p = 7.5$ s).

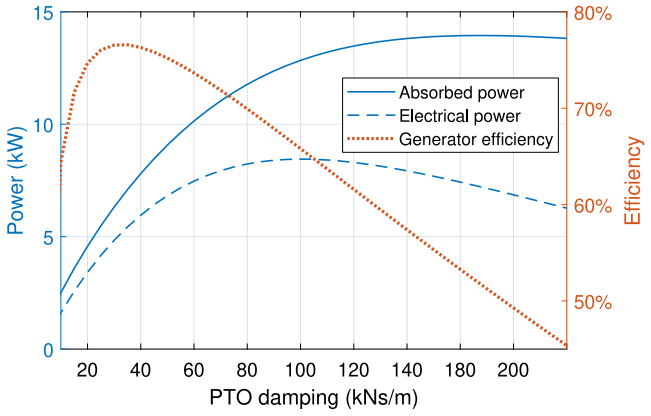

Fig. 17. The relation of the absorbed power, electrical power and generator efficiency to the PTO damping. The results are calculated by the SD wave-to-wire model. ($H_s = 2.0$ m and $T_p = 7.5$ s).

Table 2
The computational time of different models for the present case study.

Numerical modeling	FD	SD	TD
Computational time (s)	0.09	0.46	10 800+

In this case study, the PTO damping is tuned by an exhaustive search scheme for a wave state with a significant wave height of 2 m and a peak period of 7.5 s. The search boundary is defined as 10 kN m/s to 200 kN s/m with a step of 5 kN s/m. Fig. 16 depicts the relation of the power estimate of the WEC to the PTO damping. It has to be noted that, in Fig. 16, the SD wave-to-wire and TD wave-to-wire models present the grid power while the FD model could only estimate the absorbed power. It is visible that the TD and SD models result in the same optimal PTO damping, that is 100 kN s/m. Regarding the computational load, as depicted in Table 2, the SD model consumes less than 0.5 s to complete all the calculations. Comparatively, the TD model requires more than 3 h which is over 23 000 times more than that of the proposed SD model. The FD model is sufficiently fast, taking around 0.09 s. But, the optimal PTO damping searched by the FD model is 150 kN s/m, which suggests a discrepancy of 50% with regard to that obtained by the SD or TD model. This clearly implies the poor reliability of FD modeling in tuning PTO parameters to maximize the power production of WECs. The main reason can be attributed to the lack of consideration of electrical generators in FD modeling. Then the variation in generator efficiency with the PTO damping cannot be reflected.

Fig. 17 illustrates how the absorbed power, grid power and generator efficiency vary with the PTO damping, which is estimated by the SD wave-to-wire model. It is seen that the generator efficiency presents a very different trend from the absorbed power. The PTO damping maximizing the absorbed power is far from that with the highest generator efficiency. However, the actual delivered grid power is calculated as the multiplication of the absorbed power with the generator efficiency. To maximize the grid power, it is necessary to tune the PTO damping based on wave-to-wire modeling. Considering the low computational efficiency of TD models, the established SD wave-to-wire model presents satisfying performance for combining adequate accuracy and high efficiency.

6. Conclusion

In this paper, the SD modeling approach is further extended to cover the whole wave-to-wire process of WECs. A heaving point absorber equipped with a linear PM generator is considered. Multiple nonlinear effects are incorporated based on stochastic linearization in the SD model, including PTO force saturation, viscous drag force, partial overlap effect and stator current limitation. The proposed SD model is able to predict the standard deviation of the dynamic and electrical responses, overall power conversion efficiency, electrical losses and finally delivered electrical power.

The proposed SD model is verified against the results generated by a conventional TD wave-to-wire model. The achieved accuracy has a strong dependence on the intensity of the relevant nonlinear effects. Specifically, the accuracy decreases with the increased significant wave height, reduced translator length and reduced current limit. With regard to the estimated standard deviation of the stator current, the maximum relative error of the SD model to the TD model is 9%, 7% and 4.8% corresponding to a significant wave height of 4 m, a highly limited translator to stator ratio of 1.1 and a strict current limit of 130 A respectively. Regarding the power conversion efficiency, the maximum relative error is 7% and 3.2% for a significant wave height of 4 m and a current limit of 130 A respectively. Within the considered cases, the relative errors of all the estimated responses are limited to 4% where there is a significant wave height below 2.5 m, translator to stator length higher than 1.4 or the current limit is higher than 200 A. Overall, the SD model presents adequate accuracy within non-extreme most non-extreme operation or design conditions of WECs.

However, the proposed SD model is significantly faster than TD modeling with regard to computational time. With a tolerance of iterations being 0.1%, the proposed SD model is computationally faster than TD modeling in two-three orders. This clearly reflects the potential of applying the proposed SD modeling to the systematic optimization of WECs. Finally, a case study of tuning the PTO damping is carried out, in which FD, SD and TD models are used respectively. The SD wave-to-wire model predicts the same optimal PTO damping as that obtained by the TD wave-to-wire model while the computational time of the SD model is negligible compared with that of the TD model.

CRediT authorship contribution statement

Jian Tan: Conception and design of study, Acquisition of data, Analysis and/or interpretation of data, Writing – original draft, Writing – review & editing. **Wei Tao:** Conception and design of study. **Antonio Jarquin Laguna:** Conception and design of study. **Henk Polinder:** Conception and design of study, Writing – original draft, Writing – review & editing. **Yihan Xing:** Conception and design of study. **Sape Miedema:** Conception and design of study.

Declaration of competing interest

The authors declare that they have no known competing financial interests or personal relationships that could have appeared to influence the work reported in this paper.

Data availability

Data will be made available on request.

Acknowledgments

All authors approved the final version of the manuscript.

References

Anderlini, E., Forehand, D., Bannon, E., Abusara, M., 2017. Reactive control of a wave energy converter using artificial neural networks. Int. J. Mar. Energy 19, 207–220.

Babarit, A., 2015. A database of capture width ratio of wave energy converters. Renew. Energy 80, 610–628.

Balitsky, P., Quartier, N., Stratigaki, V., Verao Fernandez, G., Vasarmidis, P., Troch, P., 2019. Analysing the near-field effects and the power production of near-shore WEC array using a new wave-to-wire model. Water 11 (6), 1137.

Bárány, I., Vu, V., 2007. Central limit theorems for Gaussian polytopes. Ann. Probab. 1593–1621.

Carballo, R., Iglesias, G., 2012. A methodology to determine the power performance of wave energy converters at a particular coastal location. Energy Convers. Manage. 61, 8–18.

Ciappi, L., Simonetti, I., Bianchini, A., Cappietti, L., Manfrida, G., 2022. Application of integrated wave-to-wire modelling for the preliminary design of oscillating water column systems for installations in moderate wave climates. Renew. Energy 194, 232–248.

Coe, R.G., Bacelli, G., 2023. Useful power maximization for wave energy converters.

Cummins, W., Iiuhl, W., Uinm, A., 1962. The impulse response function and ship motions.

Delmonte, N., Barater, D., Giuliani, F., Cova, P., Buticchi, G., 2016. Review of oscillating water column converters. IEEE Trans. Ind. Appl. 52 (2), 1698–1710.

Falnes, J., 2003. Ocean waves and oscillating systems. http://dx.doi.org/10.1016/s0029-8018(02)00070-7.

Falnes, J., Hals, J., 2012. Heaving buoys, point absorbers and arrays. Phil. Trans. R. Soc. A 370 (1959), 246–277.

Folley, M., 2016a. Numerical Modelling of Wave Energy Converters: State-of-the-Art Techniques for Single Devices and Arrays. Academic Press.

Folley, M., 2016b. Numerical modelling of wave energy converters. http://dx.doi.org/10.1016/c2014-0-04006-3.

Folley, M., Babarit, A., Child, B., Forehand, D., Boyle, L.O., Silverthorne, K., Spinneken, J., Stratigaki, V., Troch, P., Folley, M., Babarit, A., Child, B., Forehand, D., Boyle, L.O., Child, B., 2019. A review of numerical modelling of wave energy converter arrays To cite this version : HAL Id : hal-01202077 A review of numerical modelling of wave energy converter arrays.

Folley, M., Whittaker, T., 2010. Spectral modelling of wave energy converters. Coast. Eng. 57 (10), 892–897.

Folley, M., Whittaker, T., 2013. Validating a spectral-domain model of an OWC using physical model data. Int. J. Mar. Energy 2, 1–11.

Fusco, F., Ringwood, J.V., 2011. Suboptimal causal reactive control of wave energy converters using a second order system model. In: The Twenty-First International Offshore and Polar Engineering Conference. OnePetro.

Garcia-Rosa, P.B., Kulia, G., Ringwood, J.V., Molinas, M., 2017. Real-time passive control of wave energy converters using the Hilbert–Huang transform. IFAC-PapersOnLine 50 (1), 14705–14710.

Giorgi, S., 2017. Linear and Nonlinear Parametric Hydrodynamic Models for Wave Energy Converters Identified from Recorded Data (Ph.D. thesis). National University of Ireland, Maynooth (Ireland).

Giorgi, G., Penalba, M., Ringwood, J., 2016. Nonlinear hydrodynamic models for heaving buoy wave energy converters.

Giorgi, G., Ringwood, J.V., 2017a. Consistency of viscous drag identification tests for wave energy applications. In: 12th European Wave and Tidal Energy Conference. pp. 1–8.

Giorgi, G., Ringwood, J.V., 2017b. Nonlinear Froude–Krylov and viscous drag representations for wave energy converters in the computation/fidelity continuum. Ocean Eng. 141, 164–175.

Giorgi, G., Ringwood, J.V., 2018. Analytical representation of nonlinear Froude–Krylov forces for 3-DoF point absorbing wave energy devices. Ocean Eng. 164 (June), 749–759.

Gonzalez, A.T., Dunning, P., Howard, I., McKee, K., Wiercigroch, M., 2021. Is wave energy untapped potential? Int. J. Mech. Sci. 205, 106544.

Gunawardane, S., Folley, M., Sanjaya, S., 2017. Spectral-domain modelling of the non-linear hydrostatic stiffness of a heaving-sphere wave energy converter. In: Proceedings of the 28th International Symposium on Transport Phenomena, Peradeniya, Sri Lanka. pp. 22–24.

Gunn, K., Stock-Williams, C., 2012. Quantifying the global wave power resource. Renew. Energy 44, 296–304.

Hals, J., Falnes, J., Moan, T., 2010. Constrained optimal control of a heaving buoy wave-energy converter. J. Offshore Mech. Arct. Eng. 133 (1), 011401.

Heath, T.V., 2012. A review of oscillating water columns. Phil. Trans. R. Soc. A 370 (1959), 235–245.

Henriques, J., Portillo, J., Sheng, W., Gato, L., Falcão, A.d.O., 2019. Dynamics and control of air turbines in oscillating-water-column wave energy converters: Analyses and case study. Renew. Sustain. Energy Rev. 112, 571–589.

Igic, P., Zhou, Z., Knapp, W., MacEnri, J., Sørensen, H., Friis-Madsen, E., 2011. Multi-megawatt offshore wave energy converters–electrical system configuration and generator control strategy. IET Renew. Power Gener. 5 (1), 10–17.

Journée, J.M.J., Massie, W.W., Huijsmans, R.H.M., 2015. Offshore hydrodynamics.

Lawson, M., Yu, Y.-H., Ruehl, K., Michelen, C., et al., 2014. Development and demonstration of the WEC-sim wave energy converter simulation tool.

Liu, C., Hu, M., Gao, W., Chen, J., Zeng, Y., Wei, D., Yang, Q., Bao, G., 2021. A high-precise model for the hydraulic power take-off of a raft-type wave energy converter. Energy 215, 119107.

Penalba, M., Cortajarena, J.-A., Ringwood, J.V., 2017a. Validating a wave-to-wire model for a wave energy converter—Part II: The electrical system. Energies 10 (7), 1002.

Penalba, M., Kelly, T., Ringwood, J., 2017b. Using NEMOH for modelling wave energy converters : A comparative study with WAMIT. In: 12th European Wave and Tidal Energy Conference. p. 10.

Penalba, M., Ringwood, J.V., 2016. A review of wave-to-wire models for wave energy converters. Energies 9 (7).

Penalba, M., Ringwood, J.V., 2019. A high-fidelity wave-to-wire model for wave energy converters. Renew. Energy 134, 367–378.

Penalba, M., Sell, N.P., Hillis, A.J., Ringwood, J.V., 2017c. Validating a wave-to-wire model for a wave energy converter—Part I: The hydraulic transmission system. Energies 10 (7), 977.

Penalba Retes, M., Giorgi, G., Ringwood, J., 2015. A review of non-linear approaches for wave energy converter modelling. In: Proceedings of the 11th European Wave and Tidal Energy Conference. European Wave and Tidal Energy Conference 2015.

Pérez, T., Fossen, T., 2008. Time-vs. frequency-domain identification of parametric radiation force models for marine structures at zero speed. Model. Identif. Control 29 (1), 1–19.

Polinder, H., 2013. Principles of Electrical Design of Permanent Magnet Generators for Direct Drive Renewable Energy Systems. Woodhead Publishing Limited, pp. 30–50.

Polinder, H., Damen, M.E.C., Gardner, F., 2004. Linear PM generator system for wave energy conversion in the AWS. IEEE Trans. Energy Convers. 19 (3), 583–589.

Polinder, H., Mecrow, B.C., Jack, A.G., Dickinson, P.G., Mueller, M.A., 2005. Conventional and TFPM linear generators for direct-drive wave energy conversion. IEEE Trans. Energy Convers. 20 (2), 260–267.

Polinder, H., van der Pijl, F., de Vilder, G.-J., Tavner, P., 2006. Comparison of direct-drive and geared generator concepts for wind turbines. IEEE Trans. Energy Convers. 21 (3), 725–733.

Prado, M., Polinder, H., 2013. Case Study of the Archimedes Wave Swing (AWS) Direct Drive Wave Energy Pilot Plant. Woodhead Publishing Limited, pp. 195–218.

Ricci, P., António, A.F., Saulnier, J.B., Pontes, M.T., 2008. Time-domain models and wave energy converters performance assessment. Proc. Int. Conf. Offshore Mech. Arctic Eng. OMAE 6 (May 2015), 699–708.

Silva, L.S.P.d., 2019. Nonlinear Stochastic Analysis of Wave Energy Converters Via Statistical Linearization (Ph.D. thesis). Universidade de São Paulo.

da Silva, L.S., Cazzolato, B.S., Sergiienko, N.Y., Ding, B., Morishita, H.M., Pesce, C.P., 2020. Statistical linearization of the morison's equation applied to wave energy converters. J. Ocean Eng. Mar. Energy 6 (2), 157–169.

Silva, L., Sergiienko, N., Pesce, C., Ding, B., Cazzolato, B., Morishita, H., 2020. Stochastic analysis of nonlinear wave energy converters via statistical linearization. Appl. Ocean Res. 95, 102023.

Son, D., Yeung, R.W., 2017. Real-time implementation and validation of optimal damping control for a permanent-magnet linear generator in wave energy extraction. Appl. Energy 208, 571–579.

Spanos, P.D., Strati, F.M., Malara, G., Arena, F., 2018. An approach for non-linear stochastic analysis of U-shaped OWC wave energy converters. Probab. Eng. Mech. 54, 44–52.

Tan, J., Polinder, H., Laguna, A.J., Miedema, S., 2022a. The application of the spectral domain modeling to the power take-off sizing of heaving wave energy converters. Appl. Ocean Res. 122, 103110.

Tan, J., Polinder, H., Laguna, A.J., Miedema, S., 2023. A wave-to-wire analysis of the adjustable draft point absorber wave energy converter coupled with a linear permanent-magnet generator. Ocean Eng. 276, 114195.

Tan, J., Polinder, H., Laguna, A.J., Wellens, P., Miedema, S.A., 2021a. The influence of sizing of wave energy converters on the techno-economic performance. J. Mar. Sci. Eng. 9 (1), 52.

Tan, J., Polinder, H., Wellens, P., Miedema, S., 2020. A feasibility study on downsizing of power take off system of wave energy converters. In: Developments in Renewable Energies Offshore. CRC Press, pp. 140–148.

Tan, J., Wang, X., Jarquin Laguna, A., Polinder, H., Miedema, S., 2021b. The influence of linear permanent magnet generator sizing on the techno-economic performance of a wave energy converter. In: 2021 13th International Symposium on Linear Drives for Industry Applications. LDIA, pp. 1–6.

Tan, J., Wang, X., Polinder, H., Laguna, A.J., Miedema, S.A., 2022b. Downsizing the linear PM generator in wave energy conversion for improved economic feasibility. J. Mar. Sci. Eng. 10 (9), 1316.

Tedeschi, E., Molinas, M., 2012. Tunable control strategy for wave energy converters with limited power takeoff rating. IEEE Trans. Ind. Electron. 59 (10), 3838–3846.

Tiron, R., Mallon, F., Dias, F., Reynaud, E.G., 2015. The challenging life of wave energy devices at sea: A few points to consider. Renew. Sustain. Energy Rev. 43, 1263–1272.

Tokat, P., 2018. Performance Evaluation and Life Cycle Cost Analysis of the Electrical Generation Unit of a Wave Energy Converter. Chalmers Tekniska Hogskola (Sweden).

Vervaet, T., Stratigaki, V., De Backer, B., Stockman, K., Vantorre, M., Troch, P., 2022. Experimental modelling of point-absorber wave energy converter arrays: A comprehensive review, identification of research gaps and design of the wecfarm setup. J. Mar. Sci. Eng. 10 (8), 1062.

Wang, L., Isberg, J., 2015. Nonlinear passive control of a wave energy converter subject to constraints in irregular waves. Energies 8 (7), 6528–6542.

Wilson, D.G., Bacelli, G., Coe, R.G., Bull, D.L., Abdelkhalik, O., Korde, U.A., Robinett, R.D., 2016. A comparison of WEC control strategies. http://dx.doi.org/10.2172/1431291.